DESIGN AND CONSTRUCTION OF A PULSED TEA/CO_2 LASER AND ITS SYNCHRONOUS COUPLING TO A RUBY LASER

GARY M. CASE

DESIGN AND CONSTRUCTION OF A PULSED TEA/CO_2 LASER AND ITS SYNCHRONOUS COUPLING TO A RUBY LASER

by

Gary M. Case, B.Sc.

Submitted in partial fulfilment
of the requirements for the degree of Master of Science
Memorial University of Newfoundland

September, 1974

ABSTRACT

A 3-metre pulsed TEA/CO_2 laser, producing 10.6 μm radiation, was constructed, and its output characteristics investigated. The laser was of the helical pin electrode configuration with nominal 1000-Ω resistors at the cathode, and thus operated in the TEM_{00} mode. The front laser window was a plane germanium mirror with 65% reflectivity, while the back window was a spherical silicon mirror with a radius of curvature of 10 m and a reflectivity of 99.4%. Input energy was supplied by a 0-30 KV power supply utilizing a triggered .03 μF capacitor which provided the pulsing mechanism for the laser. Using a gas mixture of 88% He, 6% N_2, and 6% CO_2, the peak power at 30 KV was approximately 2.4 MW and the output energy more than .5 J, effecting an efficiency of almost 4%. An image converter streak camera and a giant pulse ruby laser were simultaneously synchronized to the TEA/CO_2 laser. The purpose of this synchronization was to provide a system which could later be used to investigate stimulated ruby laser light scattering in CO_2 laser-induced plasmas. Synchronization was achieved with the aid of streak photographs of the plasmas. Plasmas in air were easily obtained using germanium lenses of focal lengths of up to 18 cm. Preliminary measurements were also made on the streak camera photographs which showed that the CO_2 laser-induced plasma expanded toward the laser with a velocity on the order of 10^6 cm sec^{-1}. Also, the size of the plasma was found to increase when the ruby laser was focused on the plasma and fired simultaneously with the TEA/CO_2 laser.

ACKNOWLEDGEMENTS

The author wishes to gratefully acknowledge the following people whose assistance made the present work possible:

Dr. C. W. Cho, for his supervision and counselling during the entire program;

Dr. H. Kiefte, for his direction throughout the project;

Dr. N. D. Foltz, for his assistance in setting up the ruby laser;

Messrs. Terry White, Adrian Walsh, and Michael Ryan, for constructing the CO_2 laser components;

Messrs. Alex McCloy and Ray Penney, for their assistance with the electronics and the synchronization;

Mr. Russ Tucker, for his assistance with the drawings in the thesis;

Mr. Ralph Alexander, for his assistance with the photography;

Miss Deanna Janes, for typing the manuscript.

The author is also indebted to his wife, Barbara, for her continuing support.

CONTENTS

LIST OF TABLES

LIST OF FIGURES

CHAPTER 1

INTRODUCTION

1-1 Development of Lasers

As early as 1950, speculation on the possible use of stimulated emission for electromagnetic wave amplification in a narrow frequency region arose [1,2]. Working with this idea, C. H. Townes and his associates conceived the first successful scheme for microwave amplification in 1954 [3,4], and applied it to the construction of a 'maser', an acronym for microwave amplification by the stimulated emission of radiation. The development of the maser then paved the way for the invention and development of the 'laser', as physicists sought to apply the stimulated emission principles to the infrared and optical regions.

Maiman's invention of the ruby laser in 1960 [5] was the first step toward the now vastly active field of laser technology. Several other solid state lasers also appeared in that year, including one of the better known utilizing neodynium glass as the laser medium.

The operation of the first gas laser also occurred in 1960 [6]. The laser medium was a mixture of helium and neon which was excited by an electrical discharge through the gas. A number of other gas lasers have appeared since 1960 and some of these will be given more detailed discussion in the next section. Semiconductor lasers appeared in 1962, followed by liquid and chemical lasers in 1963.

1-2 Gas Lasers

Gas lasers fall into three main categories according to the gas media used, the three types being atomic, ionic, and molecular. The first

atomic laser was the helium-neon laser as discussed before. Prior to the successful production of a spectral line at λ 6328 Å, in the visible region, by a helium-neon laser operating in a continuous wave mode, other noble gases were tried, but all produced infrared radiation only.

Interest mounted with the advent of the first ionic gas laser. In 1964, W. E. Bell announced the development of a laser producing visible radiation with mercury ions (Hg^+) acting as the laser medium [7]. In the same year, Bridges announced laser action in ionized argon [8]. These lasers paved the way for other ionic gas lasers, which were effective sources of high power, continuous wave red and green light.

It was in 1964, also, that the first molecular gas laser appeared, opening a new era in laser development, for molecular gases made it possible to combine efficient energy conversion with high output power. It was C. K. N. Patel who found that gas lasers would be more efficient in energy conversion if molecules, rather than the lighter atoms, were used [9]. He tried various molecular gases such as carbon monoxide, carbon disulfide, carbon dioxide, and nitrous oxide [10], but found carbon dioxide to be most efficient in energy conversion. Patel obtained energy conversion efficiencies of up to 15% with carbon dioxide in a continuous wave mode of operation, compared to efficiencies of less than 1% for atomic gas lasers.

Carbon dioxide provides radiation at λ 10.6/μm. Carbon dioxide lasers are, therefore, suitable for heating plasmas, and because λ 10.6 μm falls in the region where there is an atmospheric window, they are attractive for communications applications.

In the earlier stages of their construction for a pulsed mode of operation, carbon dioxide lasers could not produce peak powers high enough

to compete with the solid state lasers already in use. Realizing that in order to achieve such high peak powers it was necessary to keep the gas at high pressure, A. J. Beaulieu performed experiments using pressures up to an atmosphere [11,12]. However, the usual excitation technique was an electrical discharge between electrodes located at each end of the discharge tube - this meant that high voltages were necessary to break down the gas. Beaulieu solved the problem by developing a new method of excitation using transverse rather than longitudinal discharges, relative to the laser axis. Transverse excitation implies short discharge lengths and large discharge areas. The large fields necessary to break down the high pressure gas were obtained, then, with relatively low voltages applied to the electrodes.

The electrodes used by Beaulieu were a cylindrical anode and a cathode made up of a row of resistors. Using a confocal mirror configuration, such as is normally employed in longer laser cavities, Beaulieu noticed that the laser beam produced a rectangular-shaped spot [12]. He, therefore, investigated a helical electrode configuration which would favor the TEM_{00} or fundamental mode for laser oscillation. Fortin and some associates have shown that such a configuration introduces circular symmetrization of the active medium and operates reliably in this fundamental mode [13].

Considerable progress in the development of TEA/CO_2 lasers, as they are commonly known, has been evident in recent years. New electrode designs and new discharge methods have been investigated and applied, not only to the lasers using carbon dioxide gas, but to lasers using other molecular gases as well.

1-3 Statement of the Problem

The main purpose of the present work was to design and construct a three-metre long, helical TEA/CO_2 laser operating in a pulsed mode, and to investigate certain of its operational characteristics. In addition, a scheme for the synchronous operation of the CO_2 laser and a giant pulse ruby laser was undertaken in order that the CO_2-ruby laser induced plasma in a dual- or cross-beam laser field could be investigated.

CHAPTER 2

A RESUME OF THE PRINCIPLES OF AN INFRARED CO_2 LASER

2-1 Vibrational Energy Levels of Carbon Dioxide

Carbon dioxide is a linear symmetric molecule having four vibrational degrees of freedom. Associated with these are three vibrational modes which are illustrated in Fig. 1. Following the usual nomenclature for molecular vibrations [14], the first mode, the symmetric stretch mode, is designated by $(\nu_1, 0, 0)$, where ν_1 is the frequency of vibration in that mode. The second mode is the doubly degenerate bending mode which is designated by $(0, \nu_2, 0)$. The third mode, the antisymmetric stretch mode, is designated by $(0, 0, \nu_3)$.

To a first approximation, these modes are independent of one another, and the molecule can vibrate in more than one mode at a time. In other words, it may possess vibrational energy which is a combination of different modes at various vibrational quantum levels. The vibrational levels can, therefore, be written as a linear combination of the vibrational quanta v_1, v_2, and v_3, where v_1 is the vibrational quantum number of the symmetric stretch mode, and so on. Since the bending mode is doubly degenerate, it may have associated with it an angular momentum about the internuclear axis. The vibrational levels, then, are designated $(v_1 v_2^{\ell} v_3)$ where 'ℓ' is the quantum number associated with the rotational angular momentum of the bending mode. Using this nomenclature, the ground state of the molecule is designated as $(00^0 0)$.

Fig. 2 is a schematic diagram of the lower vibrational levels of a carbon dioxide molecule which are considered important for the laser

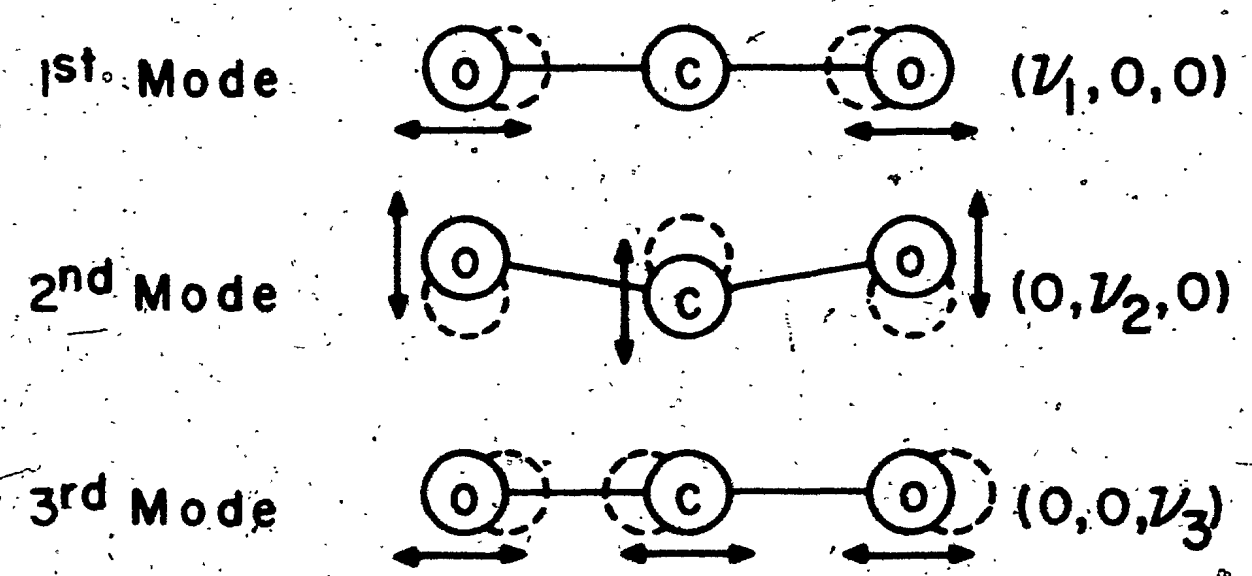

Fig. 1

The vibrational modes of a CO_2 molecule

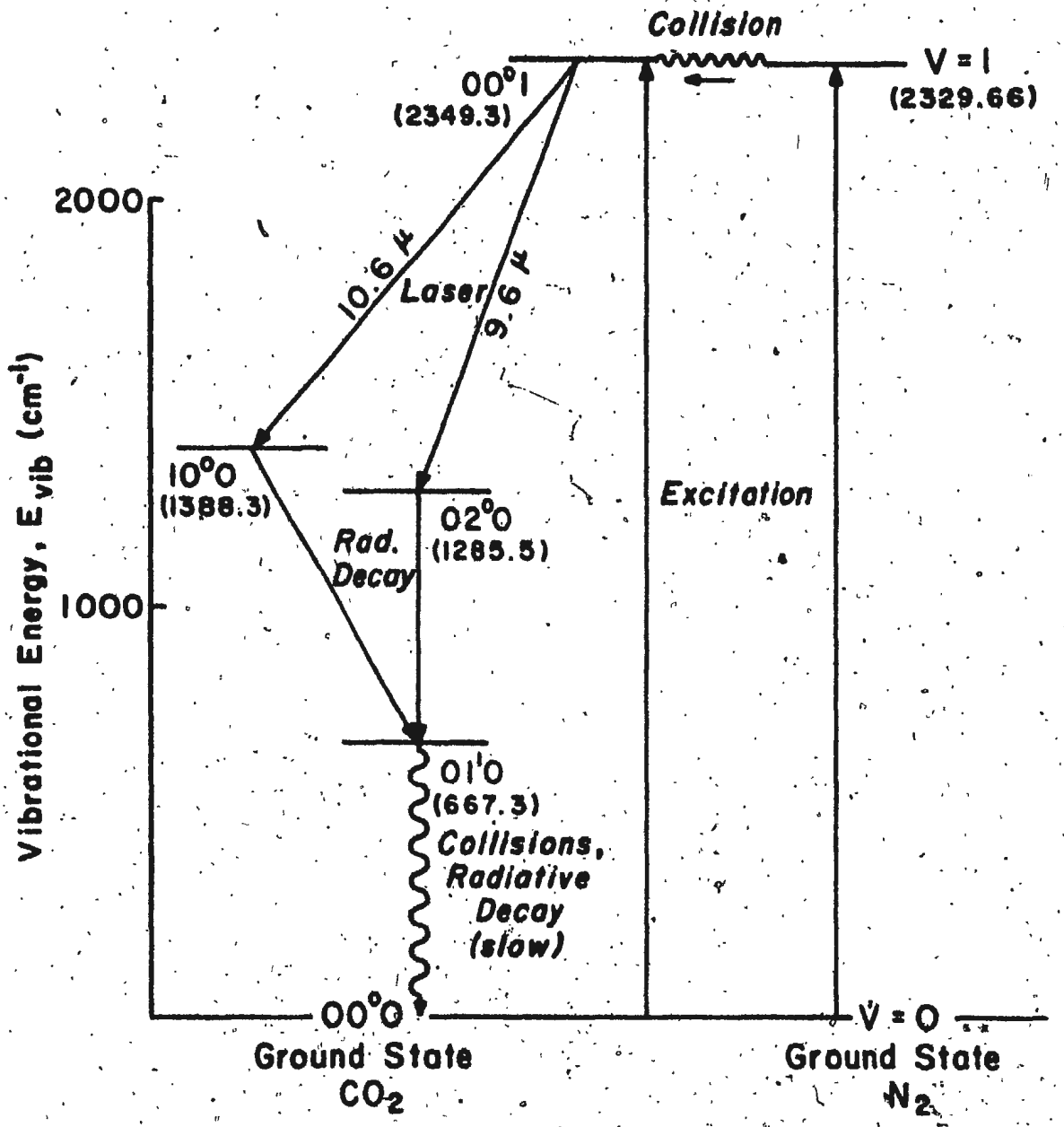

Fig. 2

Lower vibrational levels of CO_2 and N_2 molecules important for laser action

action [9]. The collisional excitation mechanism provided by nitrogen molecules is also shown in the diagram, the role of the nitrogen being discussed in detail later.

Carbon dioxide molecules are excited to the $(00^0 1)$ level by inelastic collisions between electrons and molecules as proposed by Smith and Clark [15] and shown by Boness and Schulz [16], Cheo [17], and McKnight [18]. When the $(00^0 1)$ level is populated by a majority of the molecules, in other words, when population inversion is achieved, there can be a transition to either the $(10^0 0)$ level or the $(02^0 0)$ level with infrared emission at λ 10.6 μm in the former case or at λ 9.6 μm in the latter case. Due to a greater emission probability, the λ 10.6 μm transitions are about 10 times stronger than the λ 9.6 μm transitions. The former, therefore, normally dominate and will be the only ones considered here.

Once excited to the $(00^0 1)$ vibrational level, a carbon dioxide molecule can emit a photon at λ 10.6 μm during a transition to the $(10^0 0)$ vibrational level. The collisional cross section for volume quenching for the $(00^0 1)$ level is 2.86×10^{-19} cm^2 while that for the $(10^0 0)$ level is 1.62×10^{-18} cm^2 [17]. Therefore, the lower level decays more rapidly than the upper level, so the population inversion can be expected to develop until the laser action occurs. This is a major reason why these levels are considered to be favourable laser levels.

From the $(10^0 0)$ level, the molecules decay to the $(01^1 0)$ level by collisions and *fast* radiative decay, then to the ground $(00^0 0)$ level by further collisions and *slow* radiative decay [19].

The working efficiency of a laser is related to the quantum efficiency of the transitions involved, the quantum efficiency being the highest theoretical efficiency of the laser. It is defined as the ratio of the emitted photon energy to the excitation energy. For carbon dioxide, the quantum efficiency of the $(00^0 1) - (10^0 0)$ transition is about 41% as compared to quantum efficiencies of only about 1% to 10% for typical non-molecular lasers.

2-2 Selective Excitation Mechanisms

A d.c. electric discharge through the gas results in the creation of free electrons with some kinetic energy. Direct impact between the electrons and the carbon dioxide molecules can cause the molecules to be excited to various vibrational levels. Since the $(00^0 v_3)$ levels, with different values of v_3, are nearly equally spaced, selective excitation of the molecules to the $(00^0 1)$ level is possible. A molecule at a $(00^0 v_3)$ level, $v_3 > 1$, may efficiently transfer energy to a molecule at ground $(00^0 0)$ level. The result would be a $(00^0 v_3 - 1)$ molecule and a $(00^0 1)$ molecule. Similar processes can bring other ground state molecules up to the $(00^0 1)$ level and other $(00 v_3)$ molecules down to the (001) level.

It has been found [20] that the excitation of carbon dioxide molecules to the $(00^0 1)$ level may be greatly enhanced by the addition of nitrogen gas. Since nitrogen is a homonuclear, diatomic molecule, it has no permanent dipole moment. Therefore, excited nitrogen molecules cannot decay to the ground state by means of the usual electric dipole radiation. Also, the vibrational states of the nitrogen molecule are nearly coincident with the carbon dioxide $(00^0 v_3)$ levels, as seen in Fig. 2. Accordingly,

efficient energy transfer from excited nitrogen molecules to non-excited carbon dioxide molecules can likely take place. The carbon dioxide molecules can then redistribute their energy to the $(00^0 1)$ level as described above.

The schematic representation of various processes for excitation of carbon dioxide molecules to the $(00^0 1)$ level in pure carbon dioxide and carbon dioxide-nitrogen mixtures is illustrated in Fig. 3.

2-3 De-excitation Mechanisms

Collisions of a resonant nature play an important role in the de-excitation of the carbon dioxide molecules at the $(10^0 0)$ vibrational level. The energy of the molecules at this level is approximately twice the energy of the molecules at the $(01^1 0)$ level. Consequently, collisions between two molecules, one at the $(10^0 0)$ level and the other at ground $(00^0 0)$ level, can probably result in a redistribution of the molecular energies to the $(01^1 0)$ vibrational energy level. The rate of decay of the $(01^1 0)$ level is, however, a major factor in determining the efficiency of the overall process. The vibrational energy of the molecules at the $(01^1 0)$ level may normally be lost by nonresonant collisions with the container walls or other molecules.

The addition of helium seems very effective in aiding the depletion of the $(01^1 0)$ level [21,22]. A carbon dioxide molecule undergoes about 200 collisions per second per torr at room temperature, whereas a helium atom undergoes 4000 collisions per second per torr. Helium, therefore, can contribute to increasing the overall efficiency of the laser process. The processes for de-excitation of carbon dioxide are illustrated schematically in Fig. 4.

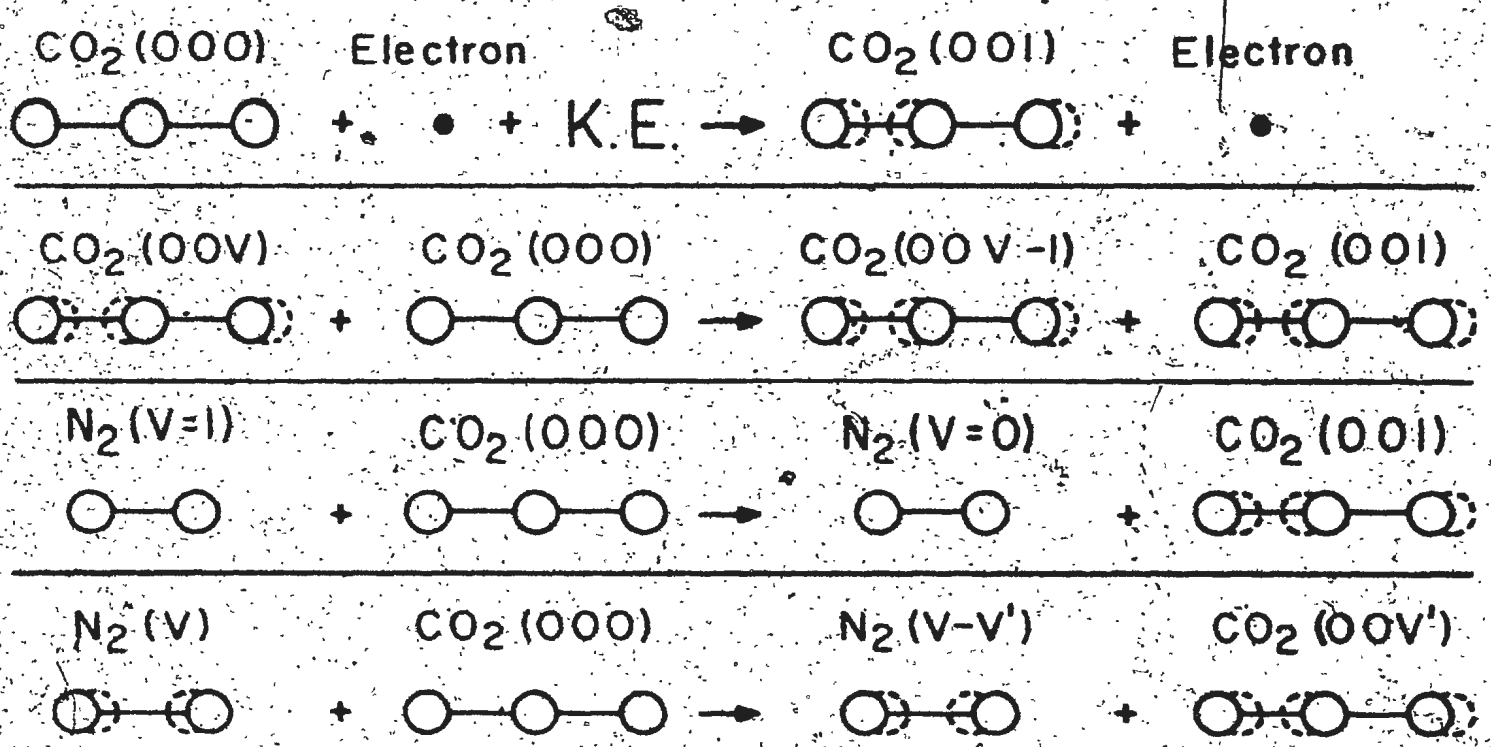

Fig. 3

Mechanisms for the excitation of CO_2 molecules to the (001) level

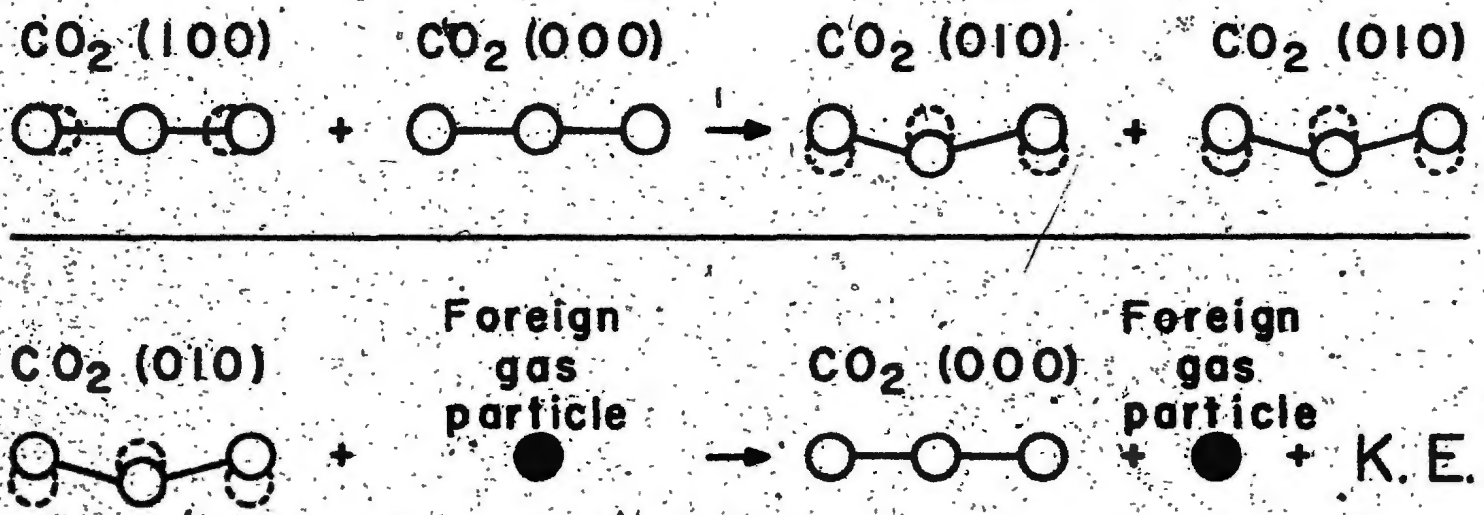

Fig. 4

Mechanisms for the de-excitation of CO_2 molecules from the (100) level to the ground (000) level

In summary, then, experimental results seem to suggest that excitation of carbon dioxide molecules to the upper laser level in pure gas is not sufficient to effect high laser efficiency. In order to enhance this excitation and to ensure greater population of the upper laser level, nitrogen can be added. On the other hand, helium can be added to the laser gas to hasten depletion of the lower laser level.

2-4 Rotational Structure of the Vibrational Levels of CO_2

Vibrational levels are made up of various rotational levels which produce P, Q, and R branch transitions for which $\Delta J = -1, 0, +1$, respectively, where J is the rotational quantum number. For carbon dioxide there are no Q branch transitions between the laser levels since ℓ, the quantum number associated with the rotational angular momentum of the bending mode, equals zero for each level. On the other hand, there may exist many possible P and R branch transitions, each producing radiation at a different wavelength. If laser output occurred along several of these transitions, then the laser light would not be truly monochromatic. This, fortunately, is not the case.

Laser action occurs along one particularly strong P branch transition. It has been shown [22] that of the observed P branch transitions the P(20) line is the most intense. The wavelength of the output radiation along this transition is 10.5915 μm.

CHAPTER 3

DESIGN AND CONSTRUCTION OF THE LASER

3-1 Mechanical Construction

The body of the laser is three metres long and is made from two equal lengths of plexiglass tube which are joined so as to form a vacuum-tight chamber. The inside diameter is approximately 4.4 cm and the outside diameter is approximately 5.1 cm. The electrode pins are arranged in a helical configuration about the tube, and are transverse to the laser axis. A schematic illustration of the electrode arrangement for the laser tube is shown in Fig. 5. Each of the cathode electrodes is a carbon resistor, one of its leads serving as the electrode pin. The pin is cut to the appropriate length and ground smooth at the point. Each cathode resistor is of 1000-Ω, ½-W size, with a maximum tolerance in the value of the resistance of ±5%, quoted by the manufacturer. Although anode electrodes of straight copper wires, as illustrated in Fig. 5, were used in an earlier prototype, carbon resistors of 2.7-Ω, ½-W size, later replaced these wires in order to ascertain accurately the length of the anode pin. Each cathode pin is located directly opposite an anode pin with a gap of 2.54 ± 0.01 cm between them. The pins are fitted into pre-bored holes and held securely in place with Lepage's epoxy to ensure a vacuum-tight seal. There are 454 electrodes of each type, and they are arranged in a helix of pitch L = 23 cm.

Each series of electrodes is connected in parallel with heavy braided wire which can easily carry high instantaneous currents. An estimated value for the maximum current through the connecting wire, as calculated in section 3-3, is about 450 amperes.

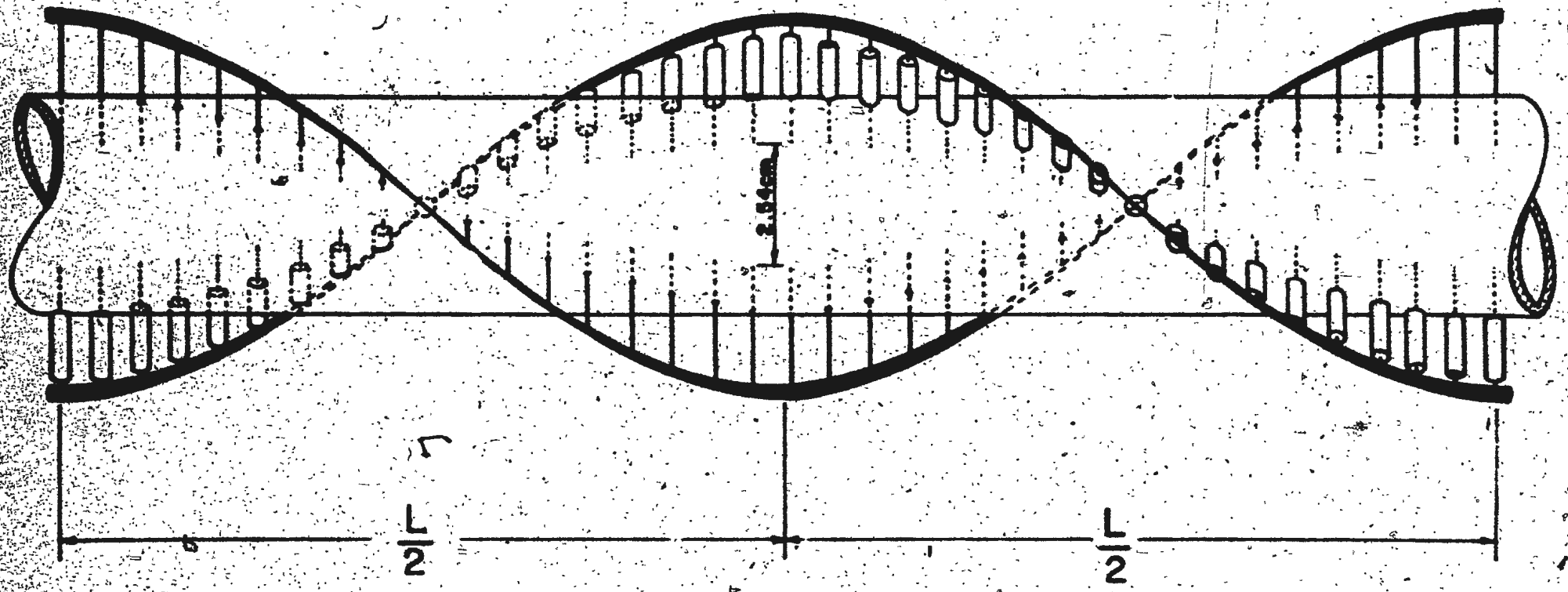

Fig. 5

Section of laser tube illustrating the electrode configuration

In a preliminary work on the construction of a TEA/CO_2 laser carried out in this laboratory, a major difficulty encountered was designing a suitable laser mount to provide the required rigidity for the laser tube as well as for the optical components. Without it, the system was difficult to allign and would remain alligned only for short periods. Because of this, the design of a suitable mount became one of the prime objects in the present work.

Fig. 6 is a photograph of the laser and the laser table used in the present work. The four pedestals for the table are built up using heavy concrete construction blocks. Across these is placed a 1-3/8-inch thick wooden slab to which an 8-inch high, 6½-inch wide steel I-beam is securely bolted. The entire table, itself, stands on the concrete floor of the laboratory. Fastened to the steel I-beam are the laser mounts (one for each end and one for the centre of the tube) and the mirror holders.

A copper screen enclosure around one side of the laser, shown in Fig. 6, is designed primarily for the safety of the operator, and also serves as a protective casing for the laser. The copper wire screen is electrically connected to the steel I-beam, which is properly grounded.

The details of the laser mount and mirror holder at one end of the laser are illustrated in Fig. 7. The mount, G, consists of two 1-inch thick plexiglass plate sections which are bolted together to hold the laser tube securely in place. The mount is then attached to the I-beam in such a way that it allows vertical adjustment of the mount (not shown in Fig. 7). A ½-inch thick plexiglass flange, F, is cemented to the end of the tube using an acrylic cement manufactured by G. C. Electronics.

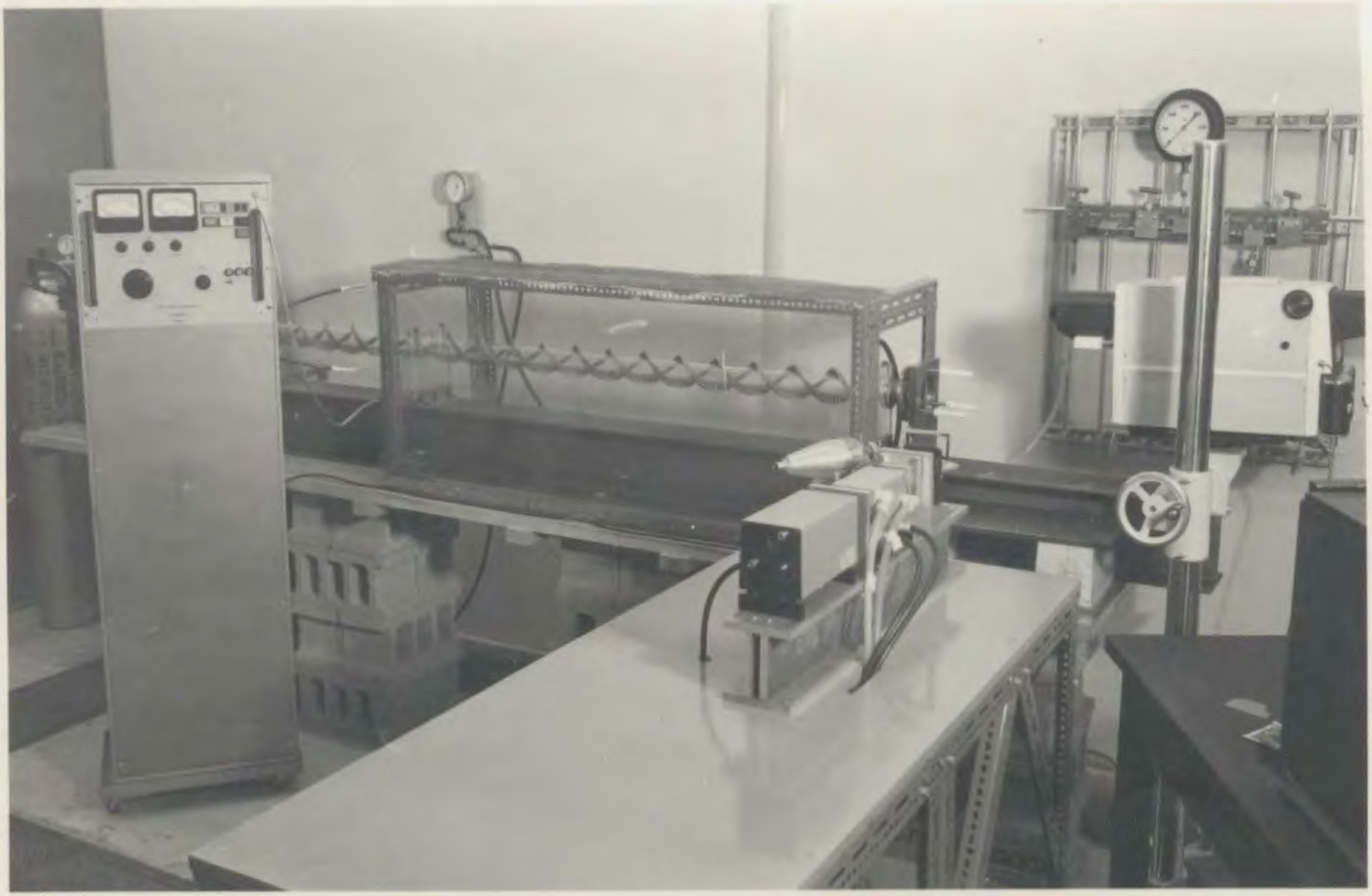

Fig. 6

CO_2 laser and associated experimental apparatus

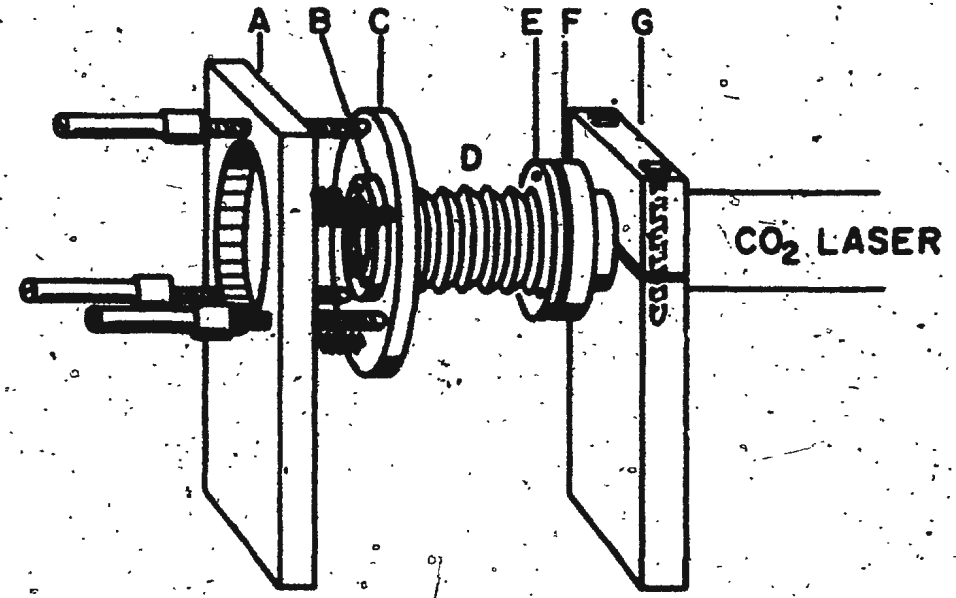

Fig. 7

Structural details of the CO_2 laser end support and mirror holder

A 3/4-inch thick brass plate, A, with a 10-cm diameter hole which is alligned concentric with the laser tube opening is bolted to the steel I-beam to serve as the end plate of the laser. The mirror holder, C, which is made from a 3/8-inch thick brass plate, has a counterbored hole into which the laser mirror fits. A teflon ring makes the seal, and the mirror is held in place by a brass ring, B. The holder, C, is attached to the end plate, A, by means of three adjusting screws and three stiff springs. The flexible brass bellows, D, one end of which is soldered to the mirror holder and the other end to a brass flange, E, permit orientational adjustment of the mirror holder. The flanges, E and F, are fastened together with an O-ring making a vacuum-tight seal. The adjusting screws attached to the plate, A, are 5/16-inch bolts with a pitch of .025 inches, and they have teflon extensions to prevent possible electrical shocks to the operator handling the screws while the system is in operation.

3-2 Optical Arrangement

The optical resonator consists of two end reflectors, one mounted at each end of the plexiglass laser tube. The back reflector is totally reflecting, while the other is partially transmitting, providing an exit for the laser beam. These reflectors were chosen so as to provide a stable focusing system. The criterion for stability, as given by Seigman [23], is

$$0 \leq g_1 g_2 \leq 1 \quad \text{(stable resonator)} \ , \tag{1}$$

where g_1 and g_2 are normalized curvature parameters associated with the output mirror and back mirror, respectively. These parameters are defined as

$$g_i = 1 - \frac{L}{R_i} \quad (i = 1,2) \ , \tag{2}$$

where L is the cavity length and R_1 is the radius of curvature of the mirror concerned. If a planar front mirror ($R_1 = \infty$) is used, i.e. $g_1 = 1$, equation (1) gives

$$0 \leq g_2 \leq 1 \quad . \tag{3}$$

For the present work a planar front reflector and a back reflector having a radius of curvature of 10 metres were used. With the valve for L being approximately 3 metres for the present laser system, the computed value for g_2 is approximately 0.7; hence, the optical system satisfies the criterion given in equation (1).

The front reflector in the present system is made of germanium plate and its front surface is coated for 65 ± 3% reflectivity at λ 10.6 μm. The back reflector is made of polycrystalline silicon plate and is coated with enhanced metal for 99.4 ± 5% reflectivity at λ 10.6 μm. Both reflectors are 2 inches in diameter and have effective apertures of 80% of the overall diameter. They were obtained from Laser Optics, Inc.

3-3 Power Supply and Related Electrical Set-Up

Input energy for the laser system is by means of fast electrical discharges across the electrodes. The energy is provided by the power supply illustrated in the schematic circuit diagram of Fig. 8. The d.c. electrical power source, manufactured by Universal Voltronics Corp., is the 32-kilovolt, 5.5-milliampere high voltage supply. C_3 and C_4 are the high voltage storage capacitors with capacitances of 0.03 and 0.01 μF, respectively. C_3 is rated for 35 kilovolts, and C_4 is rated for 50 kilovolts. The C_4 capacitor was not used in the present work. Both capacitors were made by Tobe-Deutchmann Ltd. The TM-11 Trigger, including the T-1

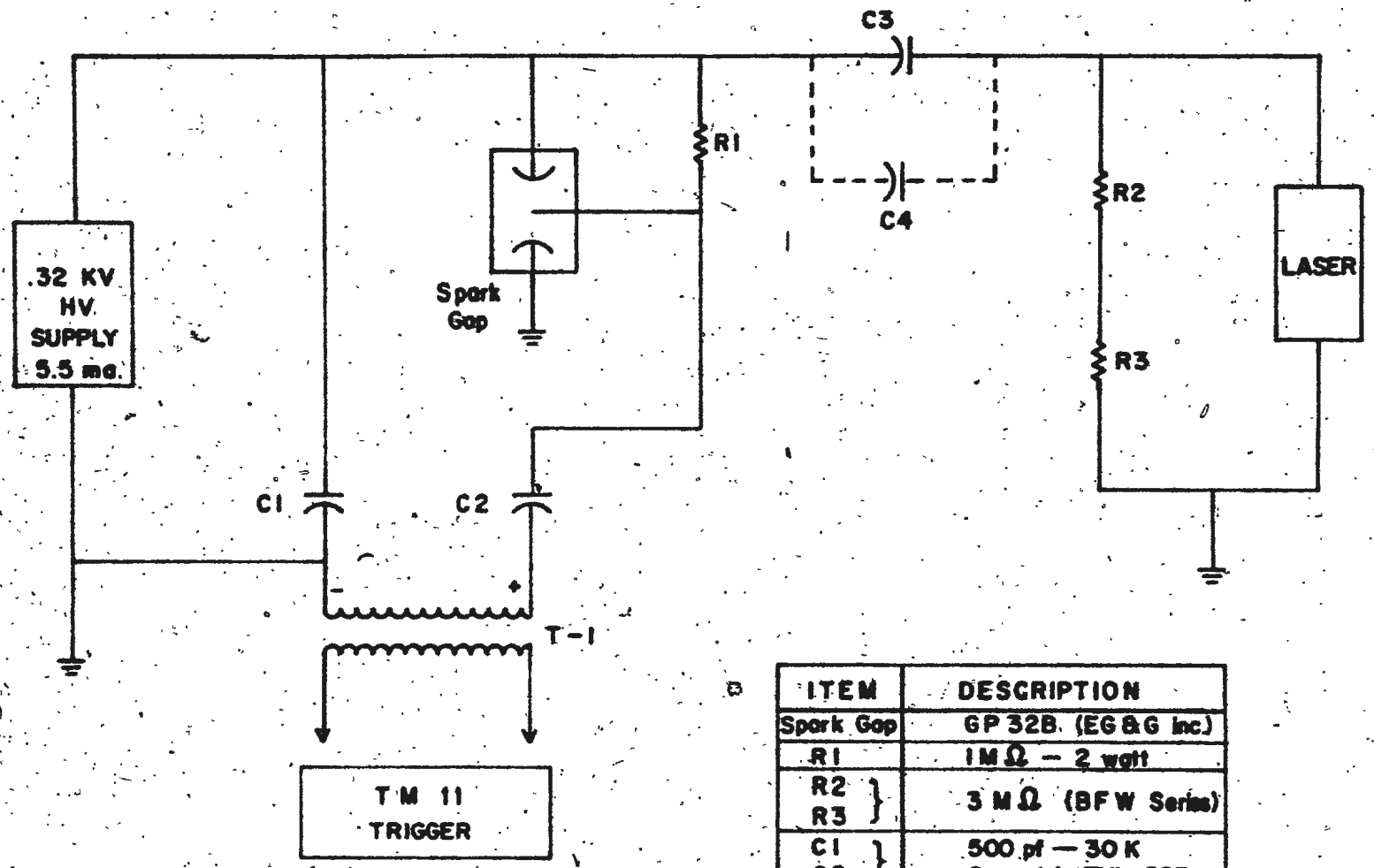

ITEM	DESCRIPTION
Spark Gap	GP 32B. (EG&G inc.)
R1	1 MΩ — 2 watt
R2, R3	3 MΩ (BFW Series)
C1, C2	500 pf — 30 K Centralab TVI-503
C3	.03 μf — 35 KV
C4	.01 μf — 50 KV
T-1	EG & G TYPE 153

Fig. 8

Circuit diagram of the CO_2 laser power supply

transformer, provides the triggering pulse to the spark gap. The spark gap, model no. GP32B, manufactured by EG and G, Inc., is the three-electrode type, having an operating range of 20 to 48 kilovolts and a static breakdown potential of 60 kilovolts.

In operation, the high voltage supply charges the storage capacitor, C_3. The adjacent electrode of the spark gap is held at high potential, while the opposite electrode is held at ground potential. A fast-rising pulse, 30-KV peak, is then generated by the TM-11 Trigger, and supplied to the spark gap trigger probe (the middle electrode in the Spark Gap of Fig. 8). The nitrogen gas which fills the spark gap is preionized and the capacitor discharges through the spark gap and across the laser. Fast electrical discharges then occur across the pin electrodes.

The full time duration, t, of these discharges is on the order of 1 μsec. A rough value for the current, I, through the braided wire connecting the electrodes can be estimated as follows: Since

$$VI \approx E/t \quad , \tag{4}$$

where V is the operating voltage and E, the total electrical energy stored in the storage capacitor, which is given by

$$E = \tfrac{1}{2} CV^2 \quad , \tag{5}$$

where C is the capacitance, then at an operating voltage of 30 kilovolts, 'I' is approximately 450 amperes.

3-4 Optical Alignment and Operation of Laser

The end mirrors are aligned using a small He-Ne laser whose mount allowed translational adjustments along vertical and horizontal axes

(perpendicular to the axis of the laser tube), as well as orientational adjustments about the same axes. The He-Ne laser is mounted on the steel I-beam at the front of the CO_2 laser. Cardboard disks with pinholes in the centres are cut to the same size as the inside diameter of the laser tube, and are used in conjunction with the line-up laser for accurate alignment of the tube sections just prior to cementing them together.

At first, the cardboard disks are placed inside the laser tube, one at each end and one at the centre where the two sections of the tube join. The direction of the line-up laser is then adjusted so that the laser beam passes through the three pinholes coincidently. The centre disk is then carefully removed and the two sections of the tube are cemented together. The end disks are then removed and the back mirror is positioned and aligned so that the line-up laser beam reflects back upon itself. The front mirror is similarly aligned taking into account a wedge in the germanium plate. Fine adjustment is done with the aid of an Optical Engineering thermal image kit, model no. 22-K, which consists of an ultraviolet lamp and a fluorescent screen. Phosphors on the screen fluoresce when illuminated by the ultraviolet lamp, but energy absorved from an infrared laser beam raises the surface temperature, producing a thermal image which appears as a dark spot on the screen.

After the laser tube is evacuated through an outlet at one end, the gas is permitted to flow in at the other end. The laser gas mixtures, obtained premixed from Matheson of Canada, Ltd., is 88% helium, 6% nitrogen, and 6% carbon dioxide. Several mixtures were tried initially but this one was found to give excellent performance for the system. Although the laser

was originally intended to be a sealed system, performance was found to be most consistent if a very slow continuous gas flow ($\approx$ 10-15 cc/sec) was allowed.

In the course of aligning the laser, an interesting effect was observed. After aligning the system and filling the tube with gas, it was sometimes necessary to remove the front mirror to check the alignment. It was then noticed that when the front mirror was removed the back mirror seemed to be out of alignment, judging from the position of the He-Ne laser beam spots. After several occurrences of the effect, the cause was discovered to be due to a variation of refractive index in the laser tube as follows: Upon removal of the front mirror, outside air flowed in under the laser gas mixture through the opening, creating a gas interface across which was a change of refractive index. The gas interface between the laser gas mixture and the outside air seemed quite stable for a considerable length of time.

As far as the stability of the present optical alignment is concerned, it has been found that even after periods of up to six months the laser remains remarkably well aligned.

CHAPTER 4

CHARACTERISTICS OF THE LASER

The planning and the painstaking attention to every constructional detail were well justified and rewarded: with just initial mirror adjustment, laser action was achieved at the first try. Using the Optical Engineering Thermal Image Kit, final optical adjustment was made. Upon focusing of the laser light with an a.r. coated germanium lens, a visible spark indicating breakdown and plasma formation in the air was observed at the focus. The repetition rate of firing of about twice a second was achieved, although the maximum rate at which the highest peak power could be maintained for each firing was observed to be about once every two seconds.

Measurements of the operational characteristics of the laser were carried out using the experimental set-up shown schematically in Fig. 9. The laser radiation detector was either a Photon-Drag Detector or a Joulemeter, depending on the characteristics being studied. A Tektronix 7704 Oscilloscope was used to analyze the signal from the detector.

At first, the Photon-Drag Detector was used to analyze the temporal profiles of the laser pulses. This detector was fabricated by the Ontario Research Foundation, Toronto, Ontario, and is especially designed for measuring the output of high-power CO_2 lasers. The main element is a germanium bar measuring 5 mm x 5 mm x 40 mm. The operational principle of such detectors has been reported by Gibson et al [24]. It utilizes the transfer of momentum from a photon beam incident on the germanium bar to electrons and holes in the metal. If sufficient momentum

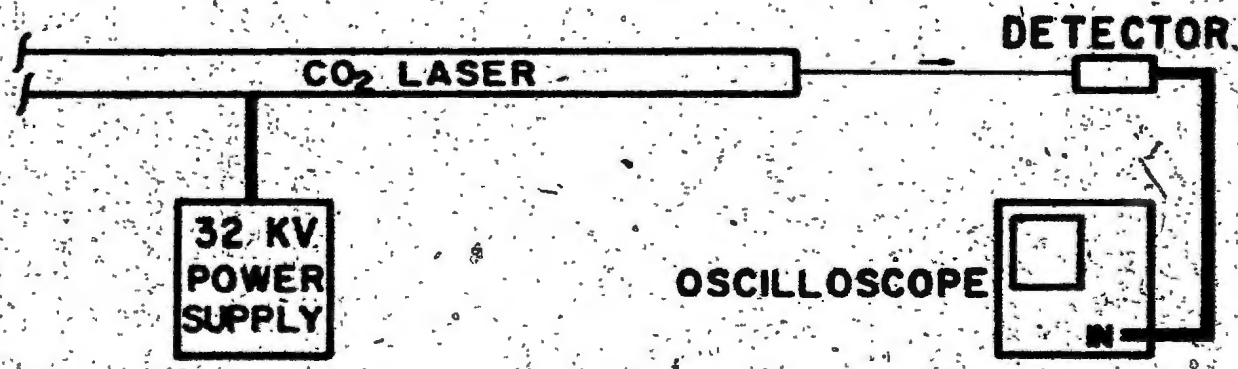

Fig. 9

Experimental setup for measurement of CO_2 laser operational characteristics

is transferred, a longitudinal e.m.f. is produced in the bar, which is then interpreted in terms of laser beam intensity by an oscilloscope.

The Photon-Drag Detector provides, essentially, pulse shapes of the laser output. Oscillograms representing typical pulses of the present TEA/CO_2 laser system are reproduced in Fig. 10. Two oscillograms in the figure show wide variations in pulse height, width, and delay, but they correspond to two different operating voltages for the laser. The top pulse was recorded with an operating voltage of 30 kilovolts for the laser or an electrical input energy of 13.5 joules to the laser, while the bottom pulse occurs with an operating voltage of 20 kilovolts or 6 joules of electrical energy.

For the present study, oscillograms of pulses were taken at 2-kilovolt intervals from 20 to 30 kilovolts applied to the electrodes of the laser. Several oscillograms were taken at each operating voltage of the laser in order to ensure a reasonable statistical validity for the pulse data. Measurements included those of pulse delay from the time the oscilloscope is triggered, temporal pulse width, and pulse height. The numerical data were obtained directly from the oscillograms using a travelling microscope.

In Fig. 11 a plot of the pulse delay versus the electrical input energy, E_i, is presented. Here E_i is calculated from the voltage, V, applied to the electrodes by means of $E_i = \frac{1}{2} CV^2$ where C is the capacitance of the storage capacitor. The oscilloscope is wired into the system in such a way that the laser and the oscilloscope are triggered simultaneously by the same switch. The delay is measured from the zero point of the oscillogram to the peak of the pulse. Since, however, it is impossible to

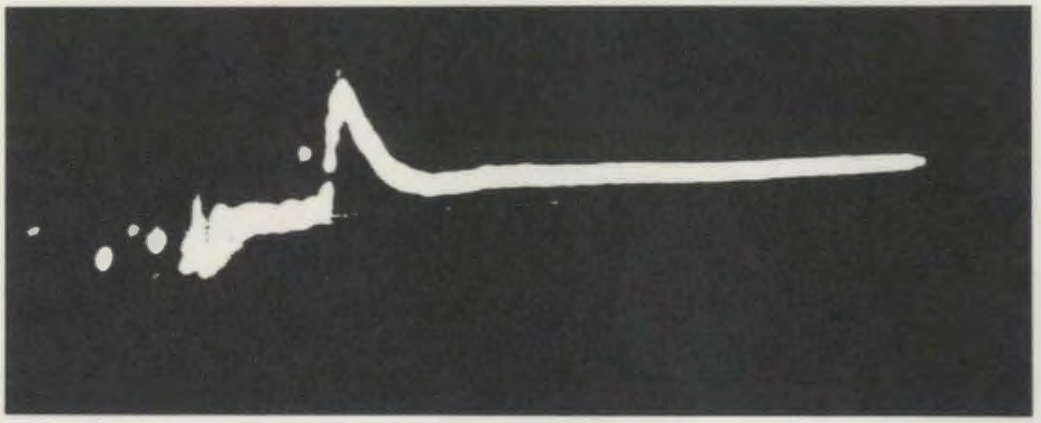

a) 30-KV pulse

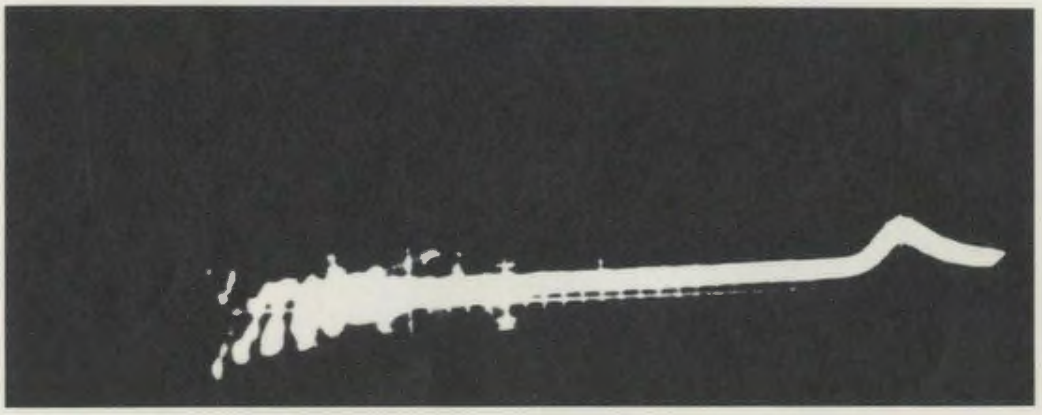

b) 20-KV pulse

Fig. 10

CO_2 laser pulse shapes

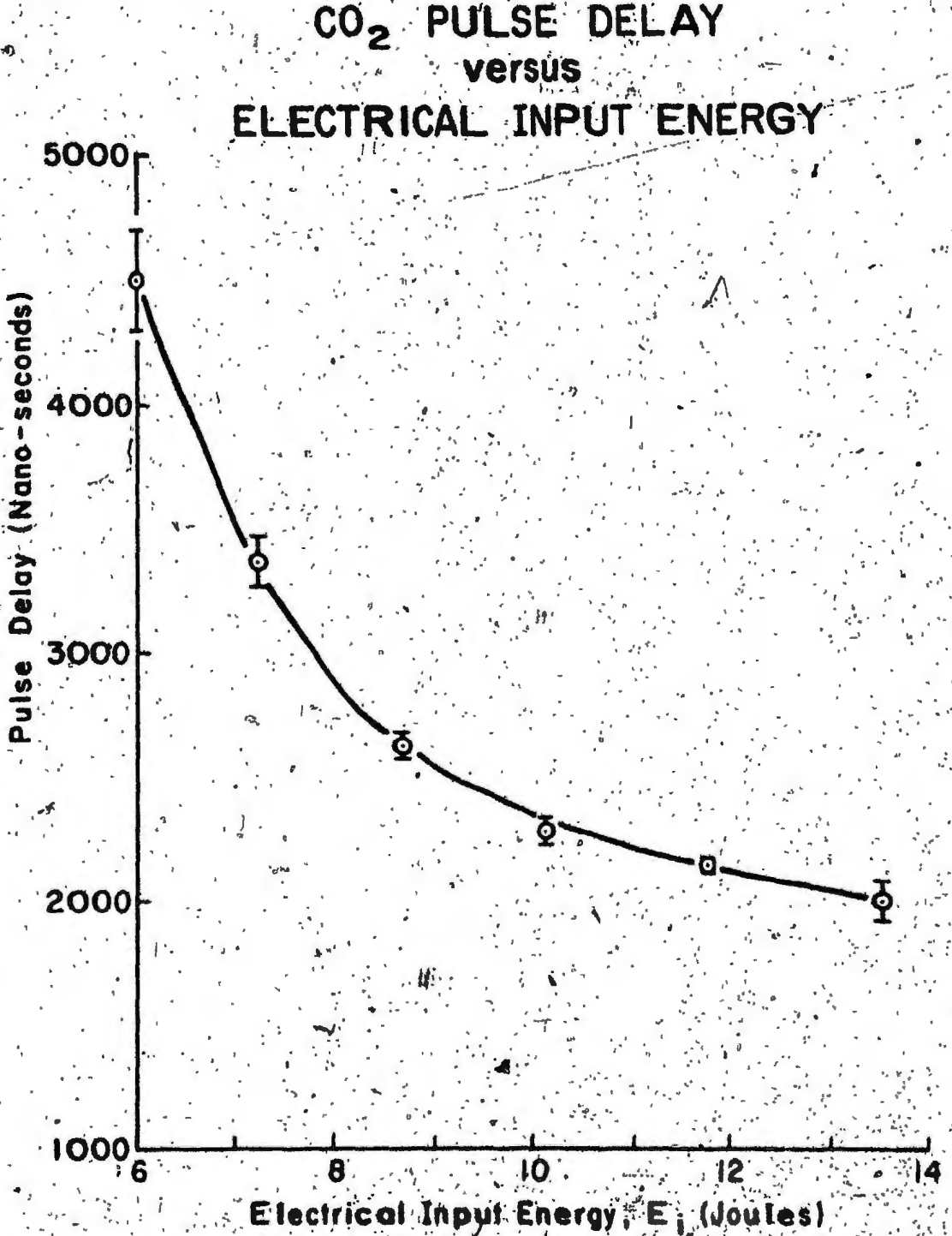

Fig. 11

CO_2 laser pulse delay versus electrical input energy

know exactly where a trace on the oscilloscope starts, an unknown but constant correction must be added to each ordinate value of the graph. The curve in Fig. 11 is drawn in free-hand. The error bars drawn for each experimental point in the diagram, as well as those in Figs. 12-15, represent the standard deviation which is computed from the measured values corresponding to a particular set of oscillograms. The spread of values at each input energy is seen from the error bars to be fairly small. The graph itself is a smooth curve and indicates a consistent increase in pulse delay with decreasing input energy, E_i.

A plot of pulse height versus E_i is shown in Fig. 12. Again, the limits of the error bars for the observed values are relatively small and a smooth curve can be drawn within the limits of the estimated error, through the averaged points. The pulse height decreases with decreasing E_i and drops off more rapidly in the low input energy region. Again, the graph is drawn in free-hand, as are all the graphs in this thesis.

The plot of the temporal pulse width at half power versus E_i is given in Fig. 13. The limits of the error bars are somewhat greater than those in the previous graphs and are greatest for low values of E_i. For the upper input energy region, the graph is nearly flat but increases sharply in the low region. The broken line indicates uncertainty as to how the curve actually falls in that region.

In each of the graphs of Figs. 11-13, the curve deviates greatest in the low input energy region. This indicates that the laser performs best from about $E_i = 8$ or 9 joules and up, or at operating voltages of approximately 24 kilovolts or greater. In this region each curve of Figs. 12 and 13 approaches a straight line, with a slope of about 43.0 $\frac{mV}{J}$

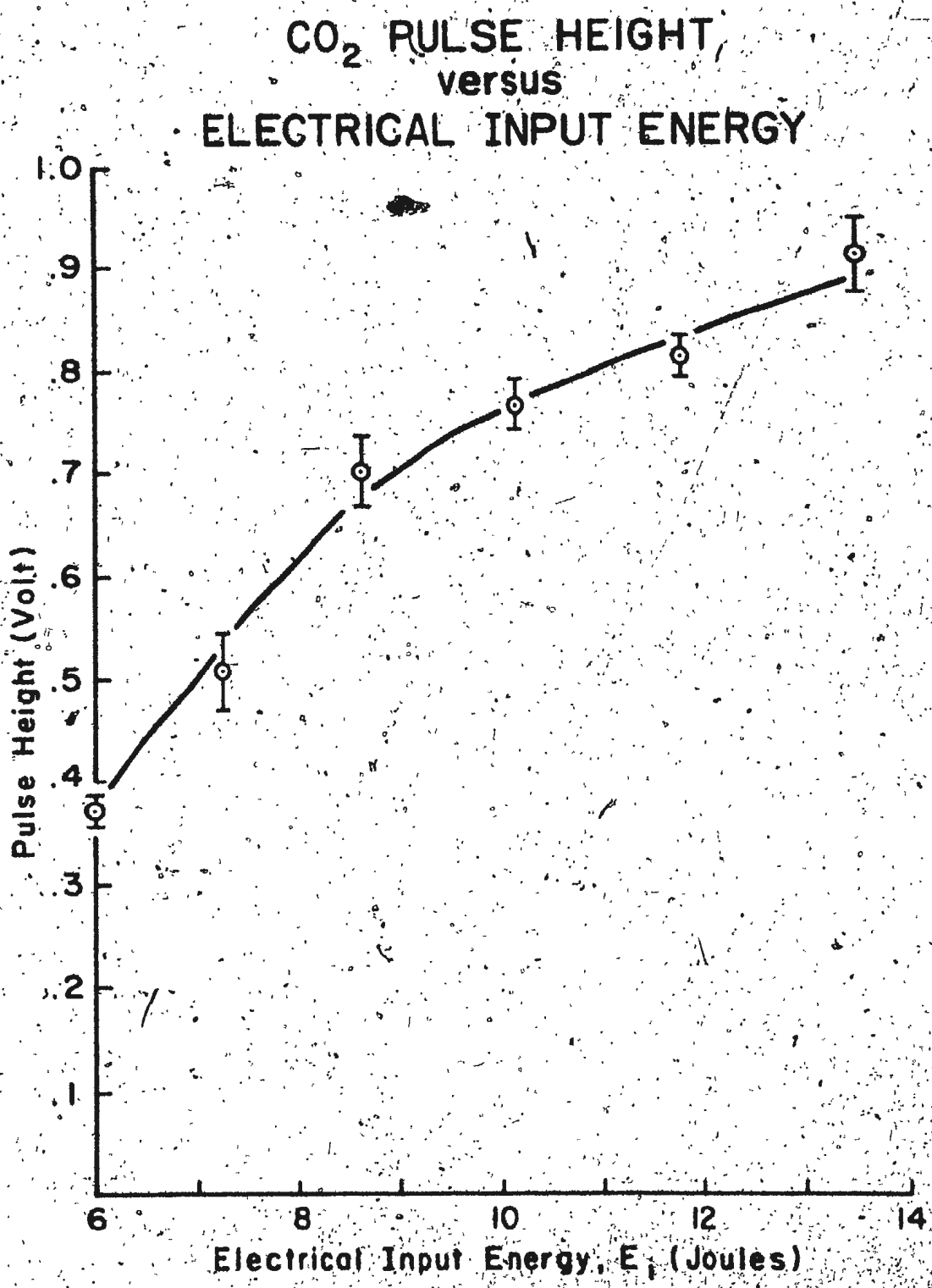

Fig. 12

CO_2 laser pulse height versus electrical input energy

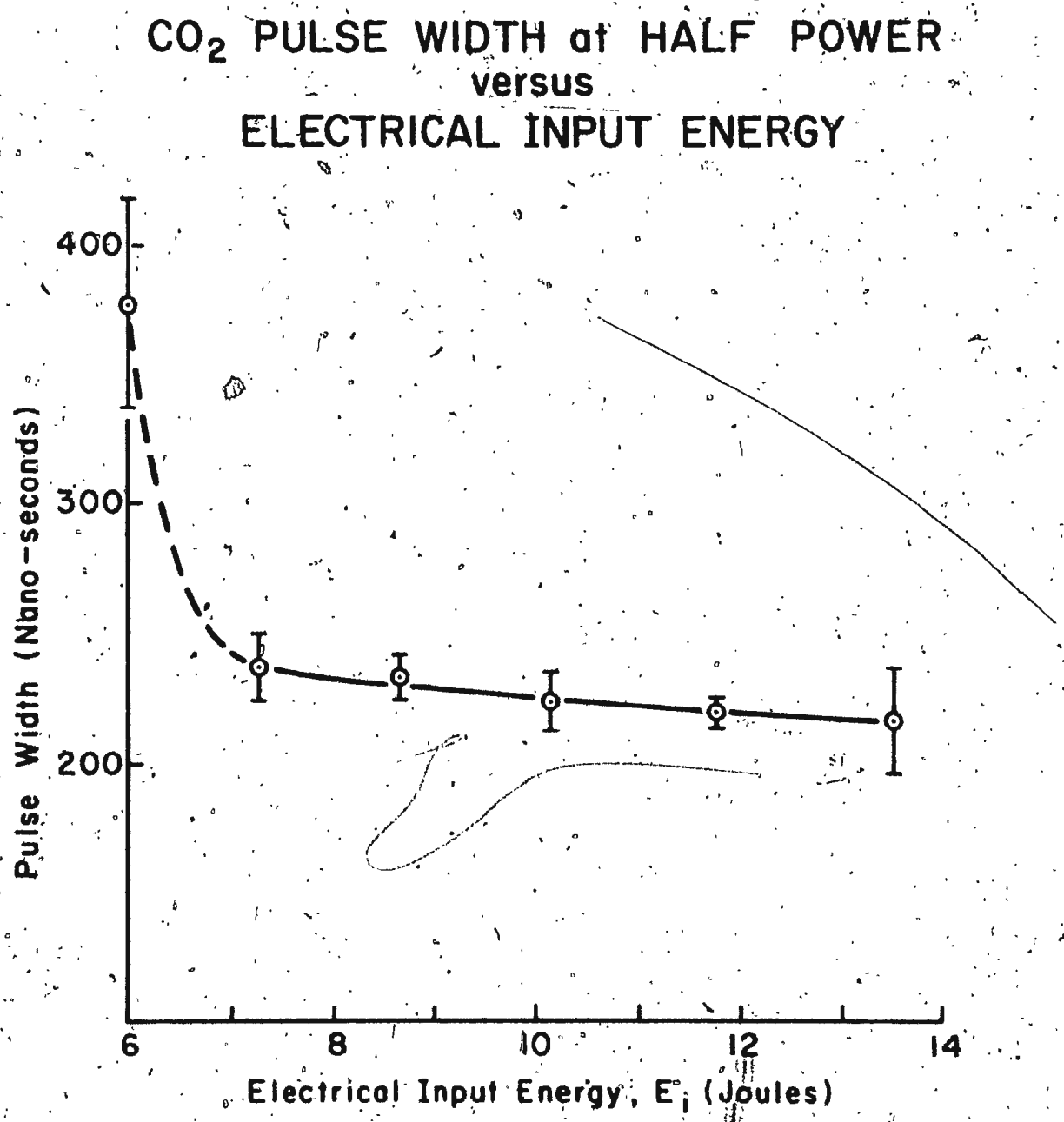

Fig. 13

CO_2 laser pulse width versus electrical input energy

for the plot of pulse height versus E_i, and a slope of about -3.2 $\frac{nS}{J}$ for the plot of pulse width versus E_i.

One of the factors most indicative of the performance of a laser is its efficiency with respect to energy conversion. This efficiency is the ratio of the measured output energy to the electrical energy, E_i, stored in the capacitor of the power supply. The output energy of the present CO_2 laser was measured using a Gen-Tec Model ED-200 Fast-Response Joulemeter. This instrument is described in the instruction manual as 'basically a current source'. Absorption of incident laser energy causes a time dependent pyroelectric current to be generated to the oscilloscope. The height of the joulemeter pulse is read in volts directly from the Tektronix 7704 oscilloscope and the reading converted to joules. From the calibration graph supplied with the joulemeter, the conversion is 9.8 volts per joule.

Fig. 14 is a plot of the CO_2 laser output energy versus the electrical input energy. The efficiencies with respect to energy conversion are also provided. The limits of error are fairly small (standard deviations again computed), and the points fall along a smooth curve. The efficiency is fairly consistent in the region above E_i = 9 joules, but begins to drop off below that.

The peak output power of the CO_2 laser is simply calculated using the formula

$$P = E_o/t \qquad (6)$$

where P is the output power, E_o, the output energy, and t, the temporal pulse width (in seconds) at half-maximum intensity. A plot of the calculated

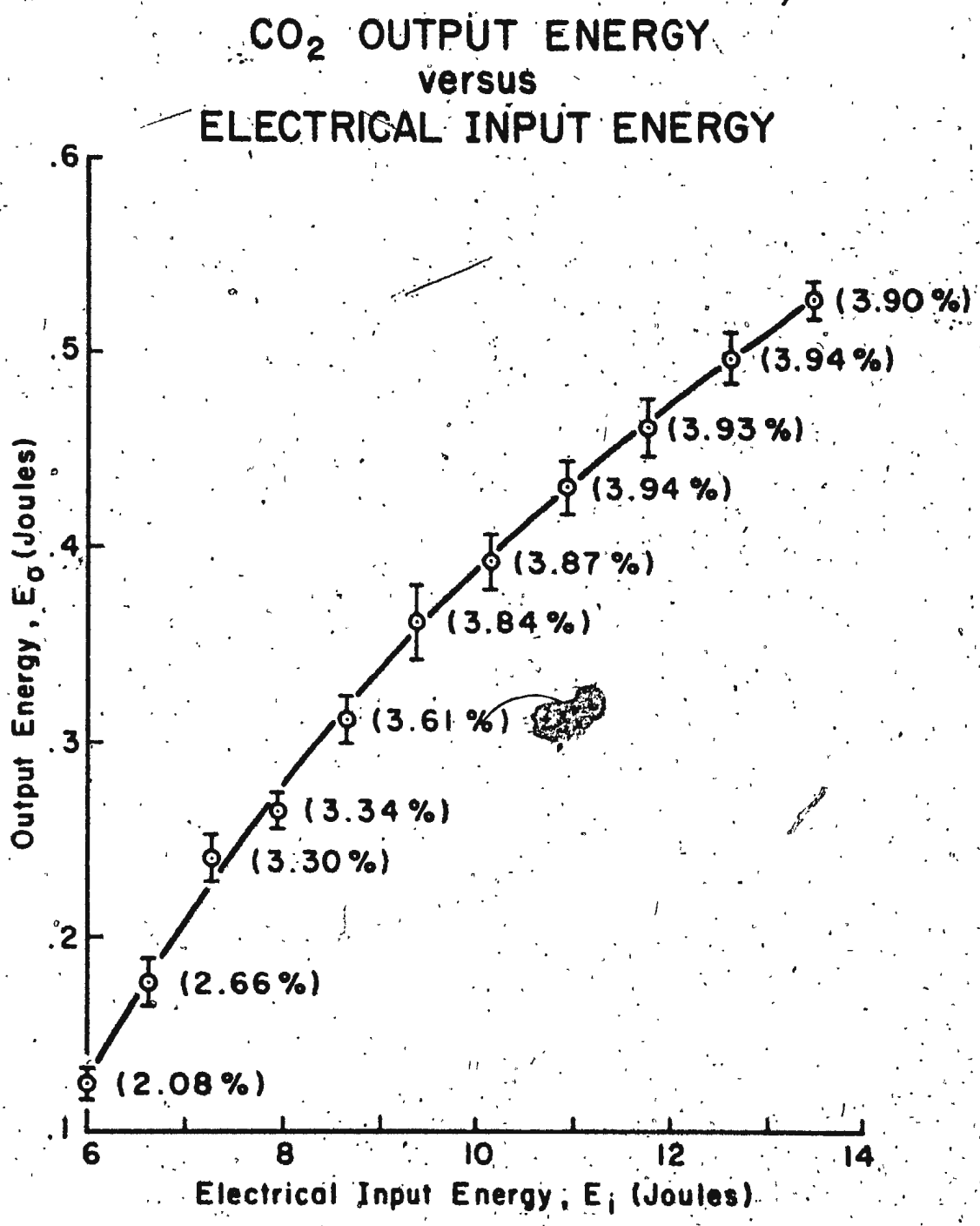

Fig. 14

CO_2 laser output energy versus electrical input energy

output power versus E_1 is shown in Fig. 15. The graph is almost a straight line except in the low E_1 region. The slope of the line is approximately $.22 \frac{MW}{J}$. The graphs of Figs. 14 and 15 again indicate that laser performance is best in the region above E_1 = 9 joules.

The major characteristics discussed are summarized in terms of slopes in Table I. Data is tabulated for two regions: the first region is from 8.5 J to 14 J, the high E_1 region, and the second is from 6-8.5 J, the low E_1 region.

The helical TEA/CO_2 laser which has been described compares quite favourably with other studies. Fortin et al [25] studied different lengths of two types of helical electrode configurations for TEA/CO_2 lasers. They obtained peak powers of about 1 MW with efficiencies of 4.1% for a 3-metre section of one electrode configuration and 2.8% for a 3-metre section of the other electrode configuration. Fortin [26] earlier obtained efficiencies of 3 to 5% and peak powers of 1 MW for a non-helical TEA/CO_2 laser. A folded path TEA/CO_2 laser studied by Laurie and Hale [27] provided a peak power of 0.2 MW with a 4.4% efficiency. Laflamme [28] has shown that double discharge systems provide greater output powers than single discharge systems. In one case he has obtained an efficiency of 7.14% at a peak output power of 4 MW, and efficiencies of 3.37% and 2.02% at a peak output power of 12 MW in two other instances.

It is considered that the TEA/CO_2 laser of the present work fully meets the requirements established at the beginning of the work, combining excellent alignment stability with high output power and good energy conversion efficiency.

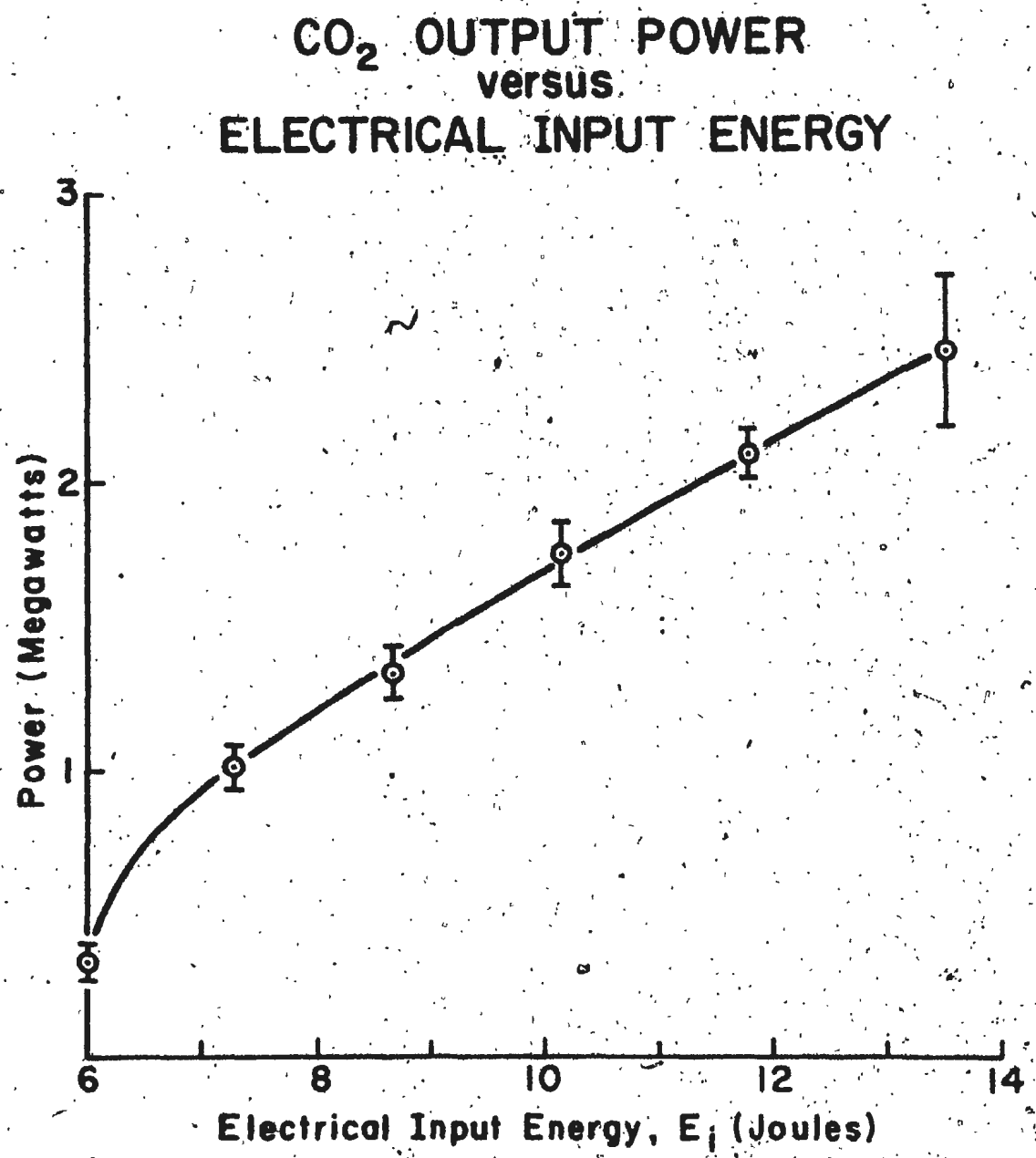

Fig. 15

CO_2 laser peak output power versus electrical input energy

TABLE I

Slopes of graphs of CO_2 laser characteristics.

Quantity	Slope (high E_i region)	Slope (low E_i region)
$\frac{\text{pulse height}}{E_i}$	43 $\frac{mV}{J}$	125 $\frac{mV}{J}$
$\frac{\text{pulse width}}{E_i}$	-3.2 $\frac{nS}{J}$	—
$\frac{\text{output power}}{E_i}$	.22 $\frac{MW}{J}$	—

CHAPTER 5

SYNCHRONIZATION OF THE CO_2 LASER TO A RUBY LASER

Having studied the characteristics of the CO_2 laser, it was decided to develop a means of synchronizing the CO_2 laser to a giant pulse ruby laser. The purpose for this exercise was to establish a future means of studying the stimulated ruby laser light scattering from a plasma. Hsu et al [29] have studied stimulated thermal Rayleigh scattering in argon, where Ar_2^* molecules are formed in a ruby laser-produced plasma. If a means, such as proposed here, of observing ruby light scattering from a previously produced plasma is established, the relation between plasma formation and light scattering can possibly be determined.

Observations of the plasma are made using an 'Imacon' image converter streak camera manufactured by John Hadland Co. The camera is focused on the plasma; when the camera is triggered, the plasma image is swept across the focal plane of the camera in a specified time interval. The time progression of the plasma during that time interval is recorded by a Polaroid camera attached to the streak camera. These time intervals range from one to ten nanoseconds per millimeter, so in order to observe the plasma consistently, it is necessary to synchronize the streak camera to the CO_2 and ruby lasers as well.

Fig. 16 is a schematic diagram of the experimental set-up. The ruby laser is electrically pumped by the 5-KV power supply. The Pockels Cell is an electronic Q-switch which is operated through the shutter control. The purpose in using the Pockels Cell is that it provides a means of triggering the ruby laser at the desired time. The thermopile, T,

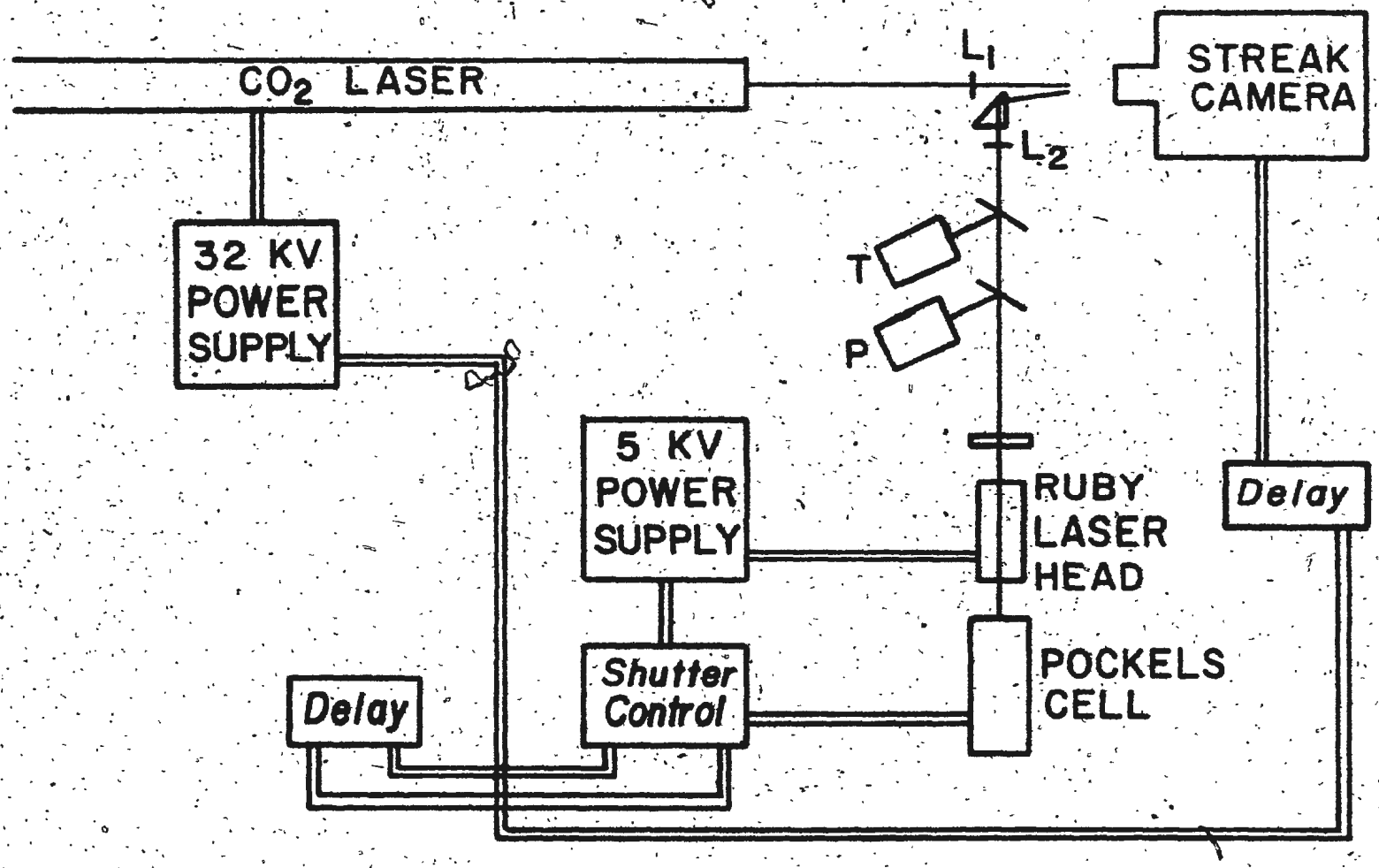

Fig. 16

Experimental setup for the synchronization of a streak camera and a ruby laser to the CO_2 laser

measures the output energy of the ruby laser, and the photodiode, P, monitors the ruby laser pulse. L_1 is an a.r. coated germanium lens of focal length 2½ inches used to focus the CO_2 laser beam, and L_2 is a glass lens of focal length 14 cm used to focus the ruby laser beam.

When the switch on the 5-KV power supply is depressed to fire the ruby laser, a signal is generated to the shutter control. The shutter control then generates signals to the CO_2 laser power supply, the Pockels Cell, and the streak camera. Since the CO_2 laser pulse delay is essentially constant for a particular CO_2 laser operating voltage, the CO_2 laser trigger is not adjusted. The signals to the Pockels Cell and streak camera, however, are delayed individually, so that triggering occurs synchronously throughout the entire system.

5-1 Observations of the CO_2 Laser-Produced Plasma

The first observations were of the plasma induced in air by the CO_2 laser only. Since the observations were made to ascertain that the CO_2 laser and streak camera were properly synchronized, the plasma was produced without any elaborate arrangements for controlling ambient conditions. Only part of the plasma can actually be observed since a slit of width 0.08 mm is used in the streak camera. The slit is centred on the plasma along the axis of the laser beam.

Shown in Fig. 17 are streak photographs of the plasma during the first several hundred nanoseconds of its time development. The top photograph was taken at an operating voltage of 30 KV, while the bottom photograph was taken at an operating voltage of 21 KV. Below 21 KV the plasma did not occur consistently.

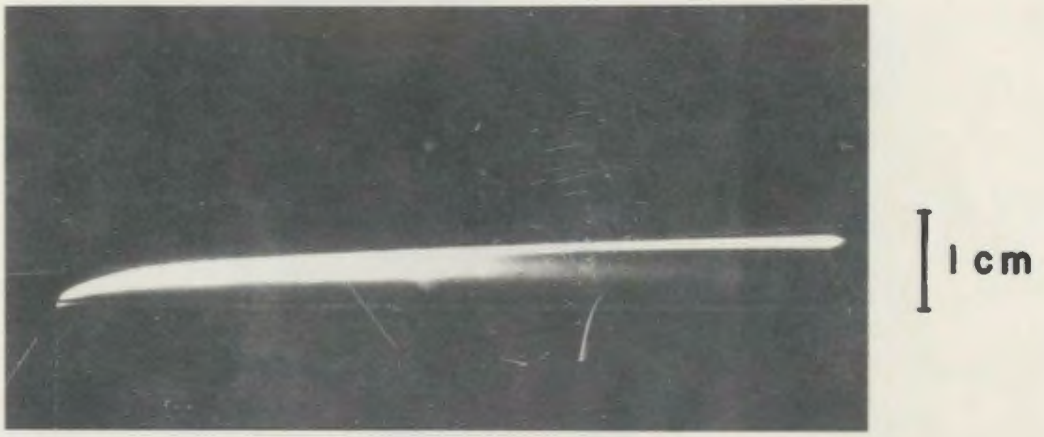

a) 30 KV

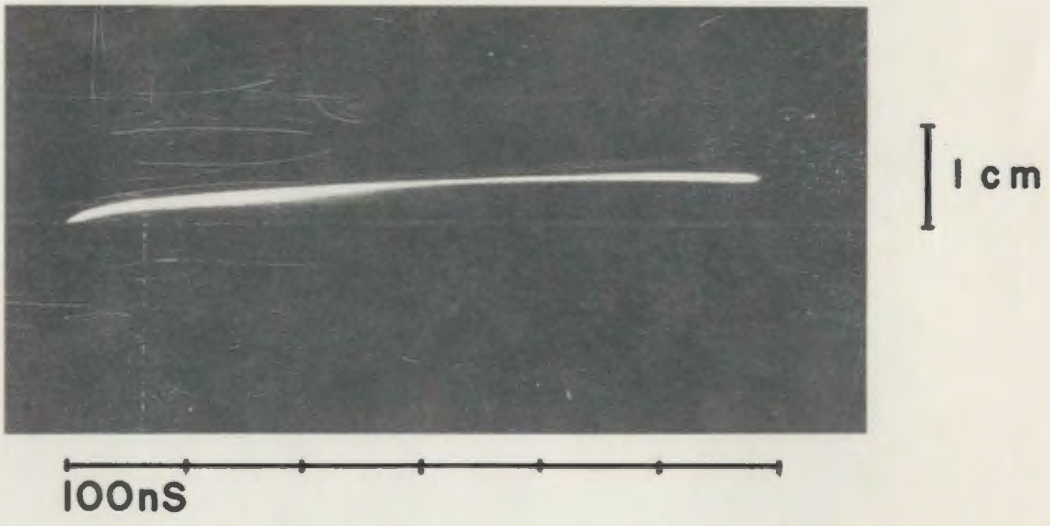

b) 21 KV

Fig. 17

CO_2 laser-induced plasma in air

The direction of the laser beam in the photographs is from top to bottom. The photographs show spatial development of the plasma from bottom to top, and time development from left to right. These observations show that the streak camera has been synchronized with the CO_2 laser, and with adjustment of the delay, different parts of the plasma can be observed.

It was decided to estimate the initial plasma velocity by obtaining measurements of distance versus time from each photograph with a travelling microscope, plotting the points in a graph, and measuring the slope of the tangent to the initial part of the curve. This was done for three sets of photographs. A theoretical calculation [30] can be obtained using the formula

$$V_{det} = \left[2(\gamma^2 - 1)\ I/\rho_0\right]^{1/3} , \qquad (7)$$

where V_{det} is the velocity of a radiation-driven detonation wave, γ, the ratio of specific heats, ρ_0, the initial density of the air, and I, the absorbed intensity. The results are presented in Table II.

Gravel et al [31] have done studies of TEA/CO_2 laser induced breakdown in air obtaining a value of $\sim 3 \times 10^6$ cm sec^{-1} for the initial plasma velocity. Tomlinson [30] has reported a lower value of 6×10^5 cm sec^{-1}. For a mode locked TEA/CO_2 laser pulse, MacPherson and Gravel [32] have reported a value for the initial plasma velocity of 6×10^6 cm sec^{-1}.

5-2 Synchronization of the Ruby and CO_2 Lasers

Approximate synchronization of the ruby laser to the CO_2 laser was first monitored with the aid of the 7704 oscilloscope. Signals from the Photon-Drag Detector for the CO_2 laser and the photodiode for the ruby

TABLE II

Estimated initial velocity of the CO_2 laser-induced plasma

Operating Voltage	E_i	Calc. Velocity ($\times 10^6$ cm sec^{-1})	V_{det}* ($\times 10^6$ cm sec^{-1})
30 KV	13.5	11.0 ± 2.9	14.1 ± 1.3
24 KV	8.64	9.98 ± 1.91	11.5 ± 0.7
21 KV	6.615	6.52 ± .27	9.7 ± 0.9

*The focused beam size, s, is calculated by [23,33]

$$S = \frac{1.22\,\lambda f}{d} ,$$

where λ is the radiation wavelength, f, the focal length of the focusing lens, and d, the lens aperture diameter. For this case, f = 6.35 cm and d = 2.2 cm; therefore, s ≈ 38 μm.

laser were monitored simultaneously by the oscilloscope. In this way, as the shutter control was being adjusted, it could be observed when both pulses coincided in time. As before, the oscilloscope was triggered externally. By means of streak photograph observations, exact synchronization could be achieved.

Fig. 18 shows streak photographs of the plasma in a dual-beam laser field. The dual-beam was created by diverting the ruby laser beam with a prism so that it travelled approximately parallel to the CO_2 laser beam, with each beam focused to the same point. The CO_2 laser was operated at a voltage of 28 KV, providing output power of about 2.1 MW. The ruby laser powar was typically from 60 to 80 MW generated in a pulse of half width of 15-20 nS. In the photographs, the ruby beam is focused on the CO_2 laser-induced plasma at different times after the plasma formation has begun. In each case, the plasma appears as before until the ruby intensity brings about a sudden change.

The following attempt was made to form a rather crude qualitative physical picture from the streak photographs. The plasma expands rapidly both forward and backward, and presumably to the sides. The sudden flair is short-lived, but leaves the plasma remaining merely as several hot spots. The effect of the ruby laser is less striking if it occurs a longer time interval after the plasma formation begins.

Observations were also done for the cross-beam laser field in which the ruby and CO_2 laser beams travel perpendicular to one another, with each beam focused to the same point. Fig. 19 shows streak photographs of the plasma in this cross-beam laser field. The first photograph from the top shows that when the effect of the ruby laser occurs very soon after

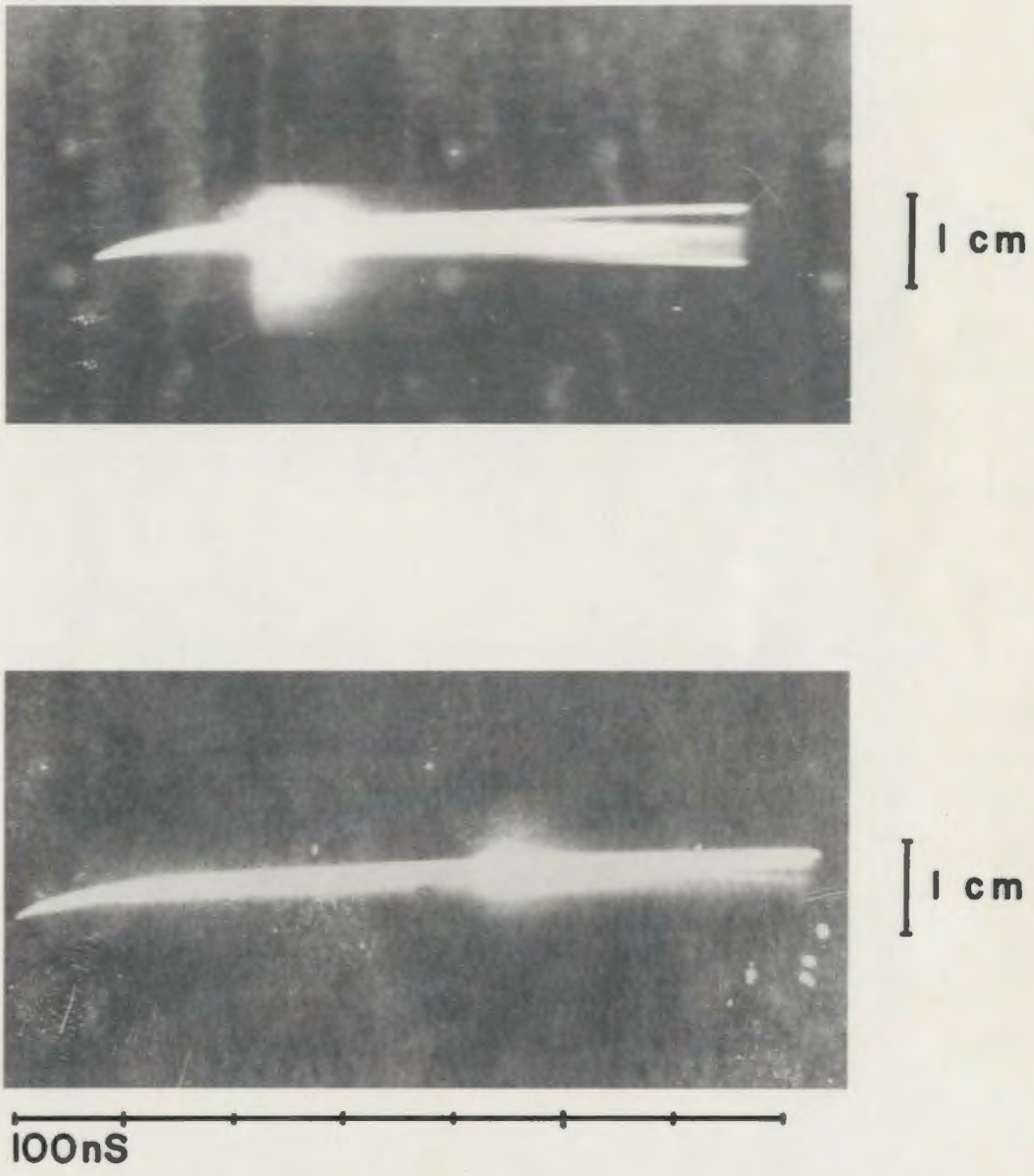

Fig. 18

Streak photographs of the plasma in the dual-beam laser field

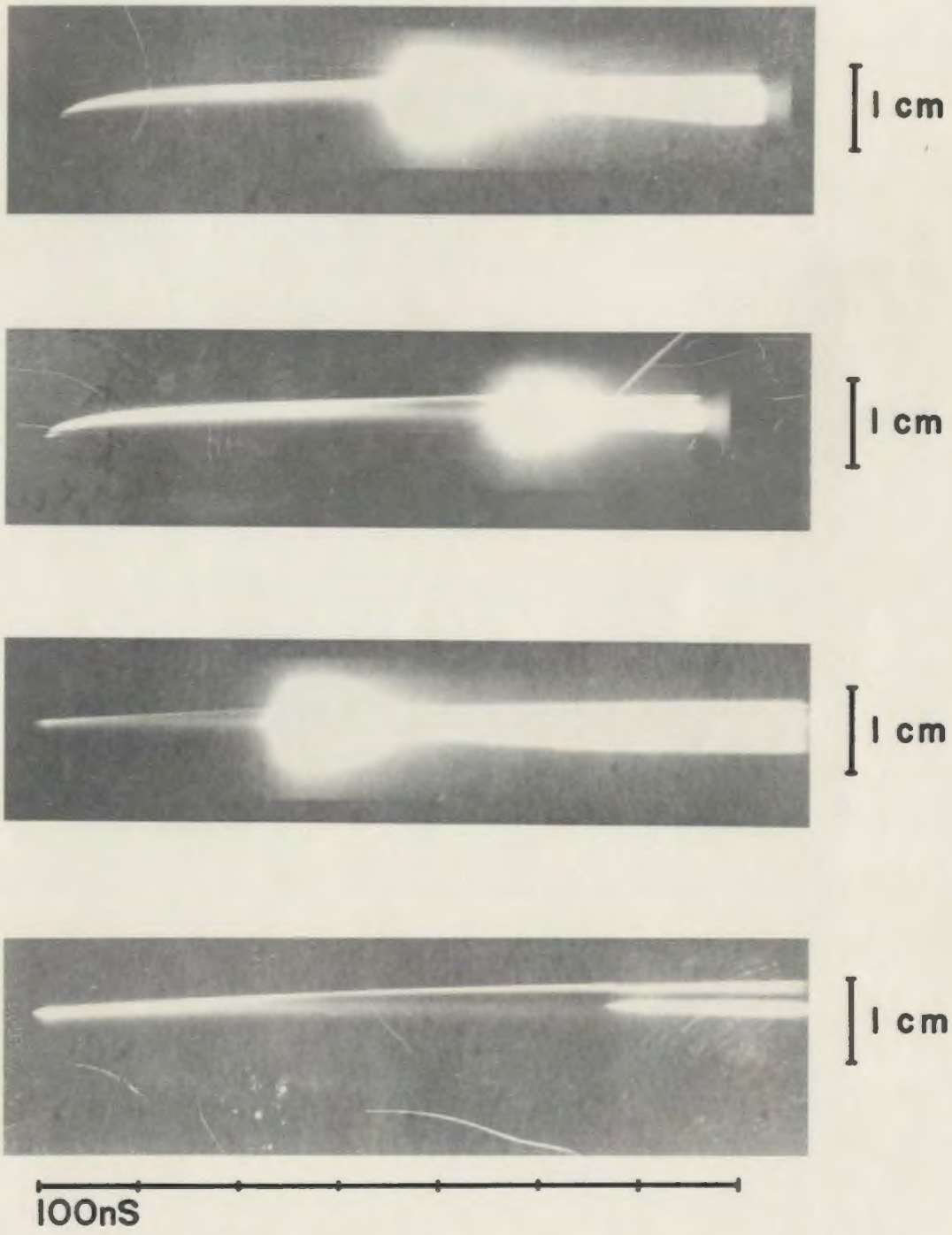

Fig. 19

Streak photographs of the plasma in the cross-beam laser field

plasma formation, the flair is somewhat longer lived than for the dual-beam case. The fourth photograph shows that the effect is noteworthy even when the plasma is almost completely decayed. Of greatest interest are the after effects. In the second, third, and fourth photographs, the plasma has been reheated by the ruby intensity and is thus longer lived. Also, the plasma front retracts somewhat, as is most easily noticed in the fourth photograph, and the revived plasma expands backward, away from the CO_2 laser, with a constant velocity and then suddenly becomes stationary. This last point of interest is most noticeable in the third photograph.

No attempt has been made to explain these effects. However, more controlled and detailed study of the interactions between the ruby laser radiation field and CO_2 laser-induced plasma, using the present system, is being undertaken at this laboratory.

To summarize, synchronization of a ruby laser to the CO_2 laser can be achieved accurately and with little difficulty with the aid of an image converter streak camera. Furthermore, interesting studies of plasmas can be done simultaneously with stimulated ruby laser light scattering experiments.

LIST OF REFERENCES

1. W. E. Lamb, Phys. Rev. 79, 549 (1950)
2. E. M. Purcell and P. V. Pound, Phys. Rev. 81, 279 (1951)
3. J. P. Gordon, H. J. Zeiger, and C. H. Townes, Phys. Rev. 99, 1264 (1955)
4. J. P. Gordon, H. J. Zeiger, and C. H. Townes, Phys. Rev. 95, 282 (1954)
5. T. H. Maiman, Nature 187, 493 (1960)
6. A. Javan, W. R. Bennett, Jr., and D. R. Herriot, Phys. Rev. Letts. 6, 106 (1961)
7. W. E. Bell, Appl. Phys. Letts. 4, 34 (1964)
8. W. B. Bridges, Appl. Phys. Letts. 4, 128 (1964); err. 5, 39 (1964)
9. C. K. N. Patel, Phys. Rev. 136, A1187 (1964)
   _____, Phys. Rev. Letts. 12, 588 (1964)
   _____, W. L. Faust, and R. A. McFarlane, Bull. Am. Phys. Soc. 9, 500 (1964)
10. C. K. N. Patel, Appl. Phys. Letts. 6, 12 (1965)
    _____, Appl. Phys. Letts. 7, 246 (1965)
    _____, Appl. Phys. Letts. 7, 273 (1965)
11. A. J. Beaulieu, Appl. Phys. Letts. 16, 504 (1970)
12. A. J. Beaulieu, Proc. of the IEEE 59, 667 (1971)
13. R. Fortin, M. Gravel, J. C. Lachambre, and R. Tremblay, Bull. Am. Phys. Soc. 15, 808 (1970)
    _____, _____, and R. Tremblay, Can. J. Phys. 49, 1783 (1971)
14. G. Herzberg, Infrared and Raman Spectra (Van Nostrand Co., Inc., N.J., 1967)
15. P. O. Clark and M. R. Smith, Appl. Phys. Letts. 9, 369 (1966)

16. M. J. W. Boness and G. J. Schultz, Phys. Rev. Letts. 21, 1031 (1968)

17. P. K. Cheo, J. Appl. Phys. 38, 3563 (1967)

18. W. K. McKnight, J. Appl. Phys. 40, 2810 (1969)

19. B. A. Lengyel, Lasers (2nd ed., John Wiley and Sons, Inc., New York, 1971), p. 356

20. C. K. N. Patel, Phys. Rev. Letts. 13, 617 (1964)

21. D. C. Tyte, Advances in Quantum Electronics, Vol. 1 (Academic Press Inc. (London) Ltd., 1970), p. 129

22. T. Laidley, M.Sc. Thesis, University of British Columbia, 1973

23. A. E. Seigman, An Introduction to Lasers and Masers (McGraw-Hill, Inc., New York, 1971)

24. A. F. Gibson, M. F. Kimmitt, and A. C. Walker, Appl. Phys. Letts. 17, 75 (1970)

25. R. Fortin, M. Gravel, and R. Tremblay, Can. J. Phys. 49, 1783 (1971)

26. R. Fortin, Can. J. Phys. 49, 257 (1971)

27. K. A. Laurie and M. M. Hale, IEEE J. Quantum Electronics, 530 (1970)

28. A. K. Laflamme, The Review of Scientific Instruments 41, 1578 (1970)

29. C. J. Hsu, N. D. Foltz, and C. W. Cho, Phys. Rev. A 9, 2365 (1974)

30. R. G. Tomlinson, Appl. Phys. Letts. 18, 149 (1971)

31. M. Gravel, W. J. Robertson, A. J. Alcock, K. Büchl, and M. C. Richardson, Appl. Phys. Letts. 18, 75 (1971)

32. R. W. MacPherson and M. Gravel, Optics Communications 4, 160 (1971)

33. S. G. Lipson and H. Lipson, Optical Physics (Cambridge University Press, London, 1969)